Article

Journal of
Nanoscience and Nanotechnology
Vol. 14, 4982–4987, 2014
www.aspbs.com/jnn

Study on the Origin of Amorphous Carbon Peaks on Graphene Films Synthesized on Nickel Catalysts

Yung Ho Kahng[1], Sung-Oong Kang[1], Gunho Jo[4], Minhyeok Choe[2], Woojin Park[2], Sangchul Lee[3], Jongwon Yoon[2], Kwanghee Lee[1,2,3,*], and Takhee Lee[4,*]

[1] *Research Institute for Solar and Sustainable Energies (RISE), Gwangju Institute of Science and Technology, Gwangju 500-712, Korea*
[2] *School of Materials Science and Engineering, Gwangju Institute of Science and Technology, Gwangju 500-712, Korea*
[3] *Department of Nanobio Materials and Electronics, Gwangju Institute of Science and Technology, Gwangju 500-712, Korea*
[4] *Department of Physics and Astronomy, Seoul National University, Seoul 151-747, Korea*

We present our investigation results on the origin of the morphological defects on graphene films synthesized by chemical vapor deposition method on nickel catalytic substrates. These defects are small-base-area (SBA) peaks with tens of nanometer heights, and they diminish the applicability of graphene films. From atomic force microscopy observations on the graphene films prepared in various ways, we found that significant portion of the SBA peaks is formed in the crevices on the nickel substrates. Our results may be useful for developing an efficient synthesis method to produce high-quality graphene films without the SBA peaks.

Keywords: Graphene, Chemical Vapor Deposition, Nickel, Morphology.

1. INTRODUCTION

The Graphene has advantageous material properties including high charge mobility, transparency, mechanical strength, and flexibility.[1,2] Accordingly, graphene is promising to be applied as a transparent electrode in electronics.[3] Currently, large-area graphene films are prepared by chemical vapor deposition (CVD) on catalytic metal surfaces.[4–6] However, CVD-grown graphene films typically show significantly high sheet resistance (100–1000 ohm/□).[3,7] Because of this poor electrical property, the wide range of potential application of CVD-grown graphene has been restricted. Given that graphene has the theoretically achievable sheet resistance of 10–30 ohm/□,[8] it is important to understand the causes limiting its electrical performance.

We have reported the existence of the morphological defects as small-base-area (SBA) peaks with tens of nanometer height in the graphene films synthesized on nickel substrates.[9]

The existence of these structural defects diminishes the applicability of the graphene films by increasing the resistance by acting as the charge scattering centers[9] and protruding through the thin active layer of the organic devices of vertical structure.[10–14] Therefore, it is important to find an efficient method to suppress the formation of the SBA peaks. And for that, identifying the origin of the SBA peaks formation on the nickel substrates during the CVD synthesis is a prerequisite.

We have reported that spike-shaped spots on the nickel substrates are the possible origin of the SBA peaks formation on the graphene films, and that the SBA peaks could be significantly decreased by decreasing the number of spike-shaped spots by etching of the annealed nickel substrates.[9]

In this report, we show that another type of morphological defects as crevices on nickel substrates form the SBA peaks on the graphene films. This finding was based on the observations that the numerous SBA peaks were formed inward of the Ni substrates and also that the SBA peaks were increased in the graphene film grown on the nickel substrates where sacrificial graphene layers

*Authors to whom correspondence should be addressed.

 1533-4880/2014/14/4982/006 doi:10.1166/jnn.2014.8411

were grown first and then removed by the plasma etching. We observed that the first growth of graphene increased the crevices, and consequently the SBA peak formation increased during the second growth of the graphene film.

2. EXPERIMENTAL DETAILS

2.1. Graphene Sample Preparation

Graphene was synthesized on Si/SiO_2 (300 nm)/Ti (20 nm)/Ni (300 nm) substrates purchased from Jinsol, Inc. Graphene films were grown on 1.2×1.2 cm^2 Ni substrates in a CVD chamber with gas flows of 208 sccm hydrogen, 192 sccm argon, and 1.4–2.0 sccm methane for 5 m at 1000 °C under 800 Torr pressure. Following synthesis, the graphene film was transferred to Si/SiO_2 substrates for characterization by etching the Ni substrate in an aqueous $FeCl_3$ solution (1 M) and washing the graphene film with distilled water. A poly(methyl methacrylate) (PMMA) coating was used as a protective layer during the transfer. More details of the synthesis and transfer has been reported elsewhere.[9]

The oxygen plasma treatments were performed in a Plasma Oxidation System, HV-100, from Hanvac, Inc. The samples were treated either for 6 m (annealed nickel substrates) or 10 m (graphene-grown nickel substrates) in oxygen plasma that was induced by a high-voltage electric source (550 V, 7 mA) in 70-mTorr oxygen.

2.2. Measurements

We used an atomic force microscope (AFM, a XE-100 system from Park Systems, Inc.) to study the morphology of the graphene films and Ni substrates. Typically AFM scans on 20×20 μm^2 areas were done at a scan rate of 0.5 Hz in the non-contact mode.

3. RESULTS AND DISCUSSION

We first investigated the change of the surface morphology of the Ni substrates, as shown Figure 1. The changes of the surface property generated with various treatments were monitored using AFM scanning. The as-produced Ni substrates show small grain sizes and numerous small peaks scattered over the area (Fig. 1(a)). When this Ni substrate was annealed with the thermal cycle of the graphene growth in the flows of 8 sccm hydrogen and 192 sccm argon, grain sizes became larger and at the same time small-numbered spike-shaped spots with the height of tens-of-nm were formed on the surface (Fig. 1(b)). Likewise, the graphene film grown with 1.6 sccm methane flow resulted in similar kinds of changes as observed in the annealed Ni substrate (Fig. 1(c)). However, in this case, some of the observed spike-shaped spots are actually the SBA peaks formed on the graphene film.

In our previous report,[9] we deduced that the SBA peaks on the graphene films are originated from the spike-shaped spots on the nickel substrate. During the graphene growth by the absorbed-carbon precipitations,[15] the carbons predominantly precipitated on the high-curvature surface areas, such as the spike-shaped spots due to the Gibbs-Thomson effect (i.e., denser precipitation on curved surfaces). In these areas, precipitated carbon may form amorphous carbon SBA peaks due to the lack of available catalyst surface to induce graphene formation.

When the annealed Ni was oxygen plasma etched, the spike-shaped spots were reduced and the protruding grains (Fig. 1(d), denoted AN-O_2P Ni) were contracted, resulting in a significant decrease of the value of root-mean-squared (rms) roughness (Fig. 1(f)). On the other hand, the rms of the graphene-grown on the Ni substrate did not decrease significantly after the oxygen plasma etching (Fig. 1(e), denoted GR-O_2P Ni). As further discussed below, such retention of the surface roughness is due to the formation of the SBA peaks within the crevices of the Ni substrates. After the removal of the graphene film, the crevices that formed the SBA peaks on graphene retained the surface roughness. And the growth of the graphene on Ni increased the formation of crevices on the Ni surface. For the statistical data shown in Figure 1(f), three samples in each condition were measured by scanning two 20×20 μm^2 areas per one sample except the as-produced Ni sample where three 20×20 μm^2 areas were scanned in one sample.

Next we discuss about the properties of the graphene films grown on the GR-O_2P Ni substrates. As we have reported in the previous report,[9] we also found that amorphous carbon lumps were formed instead of graphene when the methane flow rate is too low (Figs. 2(a)–(c)). When the methane flow rate was at 1.4 sccm or higher, the graphene film was formed (Figs. 2(e)–(f)). On the AN-O_2P Ni substrate, the graphene film did not form with the methane flow rate below 1.6 sccm. This down-shift of the threshold methane flow rate can be explained by the contribution of the absorbed carbon source during the first sacrificial graphene film growth. Because the pre-absorbed carbon source contributes to the graphene film formation in addition to the methane gas source, the grown graphene films with 1.4 sccm flows were thicker (5.5 nm) than the ones grown on the AN-O_2P Ni substrates with 1.6 sccm flows (3.6 nm) (Table I).

As previously reported,[9] these graphene films contained numerous SBA peaks as the morphological defects (the bright spikes shown in Figs. 2(d)–(f)). We counted the number of the SBA peaks on the graphene films grown with 1.4 sccm. Namely, using the threshold grain detecting function of the XEI program (Park Systems, Inc.), the domains higher than 2 nm were detected and the domains with lengths below 1 μm were counted as the SBA peaks. Previously, we have observed that the graphene film grown with the smallest methane flow rate showed the best morphology with the smallest rms roughness. For the statistical analysis, three 20×20 μm^2 areas per each sample were scanned with AFM for two samples. The results are summarized in Table I.

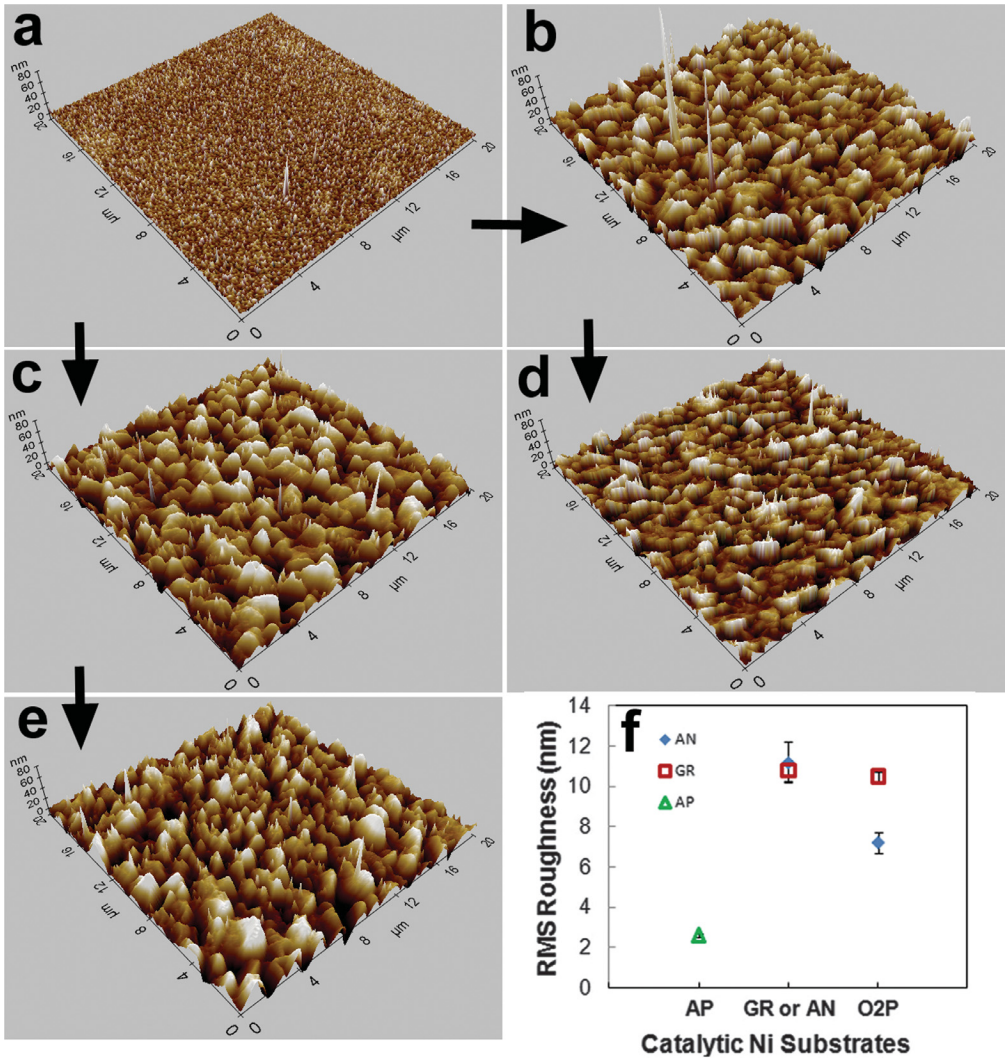

Figure 1. 20×20 μm^2 AFM images of variously treated catalytic nickel substrates of (a) as-produced (AP), (b) anealed (AN), (c) graphene-grown (GR), (d) oxygen-plasma-treated (O_2P) after AN, and (e) oxygen-plasma-treated after GR. The rms roughnesses of the nickel surfaces are summarized in (f). Note that the vertical scale (in nm unit, 80 nm max) is the same for all the AFM images.

In Table I, it can be recognized that the number of SBA peaks significantly increased on the graphene films (1.4 sccm GOG) grown on the GR-O_2P Ni substrates compared to the graphene film (1.6 sccm O_2P) grown on the AN-O_2P Ni substrates. In Table I, 1.6 sccm refers the graphene films grown on the Ni substrates without any pretreatment. From these observations, it can be deduced that the property of the Ni substrate was changed to promote the formation of the SBA peaks by growing the first sacrificial graphene film. Such change is also confirmed by the observed retention of the surface roughness of the Ni substrate even after the plasma etching of the graphene/Ni substrate (Fig. 1(f)). As shown below, we argue that this property change is the forming of many crevices on the Ni substrate.

A new origin of the SBA peaks formation on Ni was deduced from the morphology observations of the graphene films transferred with the PMMA coatings (Fig. 3); the AFM images taken on a graphene film synthesized with 1.6 sccm of methane on a Ni substrate without any pretreatment. With the PMMA coating intact, the transferred film showed somewhat retained shapes of the grains of the Ni while the SBA peaks formed outward from the Ni substrate were buried within the PMMA (Fig. 3(a)). On the other hand, when we transferred this PMMA/graphene film in a form of upside-down on a SiO_2/Si (upside-down transfer, resulting order of the layers is graphene/PMMA/SiO_2/Si), numerous SBA peaks formed inward of the Ni substrate were observable (Fig. 3(b)). These observed morphology features were confirmed to be from the graphene film

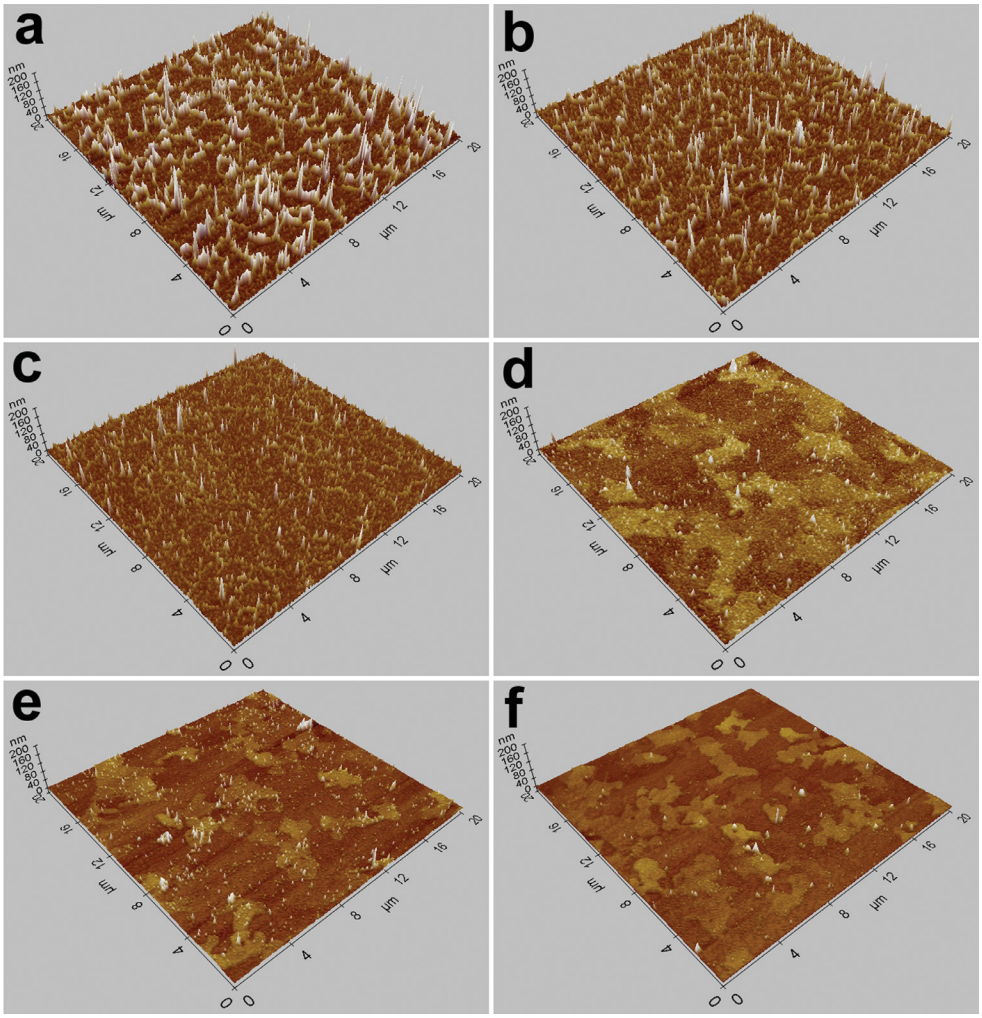

Figure 2. $20 \times 20\ \mu m^2$ AFM images of carbon films and graphene films transferred onto SiO_2/Si substrates after the syntheses with various methane flow rates of (a) 0.4, (b) 0.6, (c) 0.8, (d) 1.4, (e) 1.6, and (f) 2.0 sccm. Note that the vertical scale (in nm unit, 200 nm max) is the same for all the AFM images.

rather than from the PMMA film by observing a spin-coated PMMA film on a SiO_2/Si substrate on which a very flat surface with a couple of defects was observed (Fig. 3(c)).

This vigorous formation of the SBA peaks inward of the Ni substrate provides important information on the origin of the SBA peak formation. Because the graphene film is mainly formed by precipitation of the absorbed carbon source as the temperature decreases,[15] the inward formation of the SBA peaks must happen within the crevices on the Ni. As discussed above, these crevices can also induce dense precipitation by the Gibbs-Thomson effect to form the SBA peaks. In our previous report,[9] we observed the decreased number of the SBA peaks on the graphene films grown on the AN-O_2P Ni substrates where the spike-shaped spots were decreased compared to the graphene

Table I. Morphological characteristics of the graphene films synthesized in various conditions. Note that the data in the first two rows were reported previously by us.[9] We include them here for a comparison.

Sample	Thickness (nm)	Roughness (nm)	No. of SBA peaks	SBA peak area ($10^{-3}\ \mu m^2$)	No. of ML domains	ML domain area (μm^2)
1.6 sccm	3.4 ± 0.2	2.2 ± 0.1	729 ± 89	13.1 ± 0.5	32 ± 2	3.8 ± 0.5
1.6 sccm O_2P	3.6 ± 0.2	2.0 ± 0.1	492 ± 98	17.3 ± 1.3	23 ± 2	6.2 ± 0.9
1.4 sccm GOG	5.5 ± 0.4	3.6 ± 0.5	2380 ± 770	10.7 ± 0.8	40 ± 6	3.2 ± 0.9

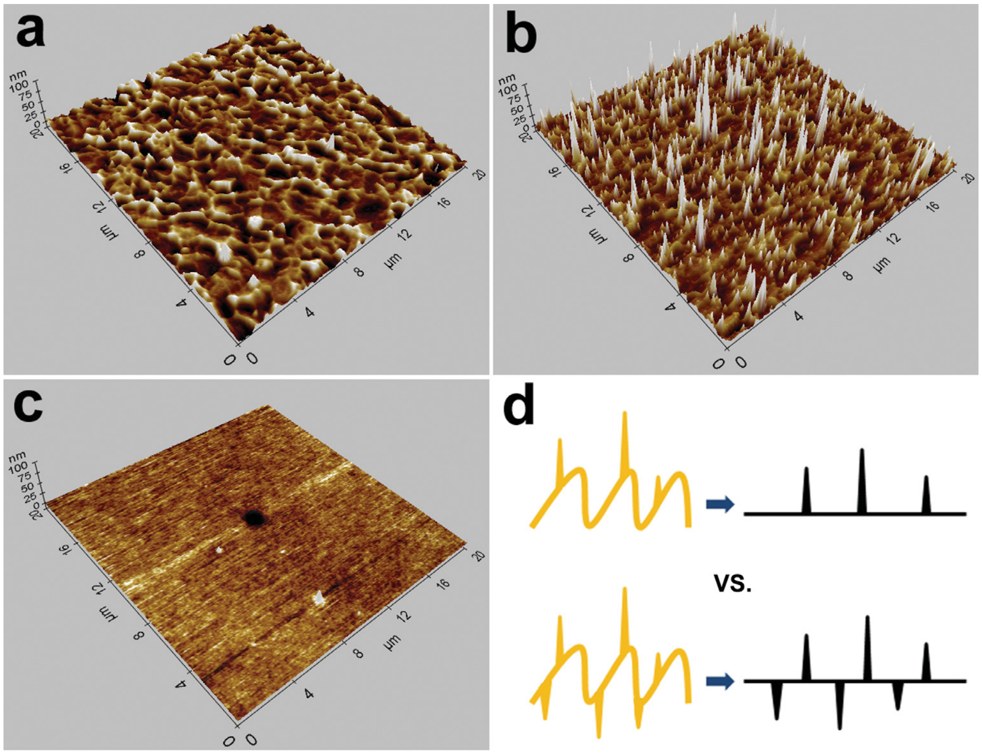

Figure 3. (a), (b) Morphology of the graphene films with PMMA coatings (thickness: ~50 nm) on SiO_2/Si substrates. (a) With normal transfer, the SBA peaks are mostly buried within the PMMA. (b) On the other hand, with upside-down transfer, the SBA peaks formed inward of the Ni surface are revealed. (c) The PMMA coating itself was flat except a few defects. These observations reveal a new origin of the SBA peaks formation as illustrated in (d).

films grown on the as-produced Ni substrates.[9] However, we observed only a 33% decrease in the number of the SBA peaks (Table I).

Based on the observations on the origin of the SBA peaks, this small reduction of the SBA peaks can be explained. Because the crevices on the Ni substrate are also an important origin for the formation of SBA peaks on the graphene films and these crevices cannot be reduced by the plasma-etching, a significant portion of the SBA peaks were still formed. In the same manner, we can explain the observations discussed above: (1) the surface roughness of the GR-O_2P Ni substrate was considerably rougher than the AN-O_2P Ni substrate because the formation of the graphene retained or perhaps increased the crevices on the Ni surface, and (2) the SBA peaks increased on the graphene film grown on the GR-O_2P Ni substrates because the more crevices existed on the surface promoting the formation of the SBA peaks compared to those grown on the AN-O_2P Ni substrates. This newly discovered origin of the SBA peak formation is illustrated in Figure 3(d).

Understanding the origin of the SBA peaks formation on the Ni substrate can be useful for finding an efficient synthesis method to suppress the SBA formation on the graphene film. Namely, the crevices on the Ni substrates should be reduced as well as the outward formation of spike-shaped spots on the Ni substrates in order to synthesize high-quality graphene films without the SBA peaks of amorphous carbon nature during the CVD process.

4. CONCLUSION

In this report, we found that the morphological defects in the form of crevices on Ni substrates play a significant role in the formation the SBA peaks on graphene films. This newly discovered origin of the SBA peaks formation may be useful to develop an efficient CVD synthetic approach for the suppression of the SBA peaks on graphene.

Acknowledgment: This work was supported by the Core Technology Development Program for Next-generation Solar Cells of Research Institute for Solar and Sustainable Energies (RISE), GIST.

References and Notes

1. A. K. Geim and K. S. Novoselov, *Nature Mater.* 6, 183 (**2007**).
2. A. K. Geim, *Science* 324, 1530 (**2009**).
3. J. K. Wassei and R. B. Kaner, *Mater. Today* 13, 52 (**2010**).
4. K. S. Kim, Y. Zhao, H. Jang, S. Y. Lee, J. M. Kim, K. S. Kim, J.-H. Ahn, P. Kim, J.-Y. Choi, and B. H. Hong, *Nature* 457, 706 (**2009**).

5. A. Reina, X. Jia, J. Ho, D. Nezich, H. Son, V. Bulovic, M. S. Dresselhaus, and J. Kong, *Nano Lett.* 9, 30 **(2009)**.
6. X. Li, W. Cai, J. An, S. Kim, J. Nah, D. Yang, R. Piner, A. Velamakanni, I. Jung, E. Tutuc, S. K. Banerjee, L. Colombo, and R. S. Ruoff, *Science* 324, 1312 **(2009)**.
7. S. Bae, H. Kim, Y. Lee, X. Xu, J.-S. Park, Y. Zheng, J. Balakrishnan, T. Lei, H. R. Kim, Y. I. Song, Y.-J. Kim, K. S. Kim, B. Ozyilmaz, J.-H. Ahn, B. H. Hong, and S. Iijima, *Nature Nanotech.* 5, 574 **(2010)**.
8. J.-H. Chen, C. Jang, S. Xiao, M. Ishigami, and M. S. Fuhrer, *Nature Nanotech.* 3, 206 **(2008)**.
9. Y. H. Kahng, S. Lee, M. Choe, G. Jo, W. Park, J. Yoon, W.-K. Hong, C. H. Cho, B. H. Lee, and T. Lee, *Nanotechnology* 22, 045706 **(2011)**.
10. M. Choe, B. H. Lee, G. Jo, J. Park, W. Park, S. Lee, W.-K. Hong, M.-J. Seong, Y. H. Kahng, K. Lee, and T. Lee, *Org. Electron.* 11, 1864 **(2010)**.
11. G. Jo, S.-I. Na, S.-H. Oh, S. Lee, T.-S. Kim, G. Wang, M. Choe, W. Park, J. Yoon, D.-Y. Kim, Y. H. Kahng, and T. Lee, *Appl. Phys. Lett.* 97, 213301 **(2010)**.
12. B. Cho, T.-W. Kim, S. Song, Y. Ji, M. Jo, H. Hwang, G.-Y. Jung, and T. Lee, *Adv. Mater.* 22, 1228 **(2010)**.
13. Y. Ji, B. Cho, S. Song, T. W. Kim, M. Choe, Y. H. Kahng, and T. Lee, *Adv. Mater.* 22, 3071 **(2010)**.
14. Y. Ji, B. Cho, S. Song, M. Choe, T.-W. Kim, J.-S. Kim, B.-S. Choi, and T. Lee, *J. Nanosci. Nanotechnol.* 11, 1385 **(2011)**.
15. X. Li, W. Cai, L. Colombo, and R. S. Ruoff, *Nano Lett.* 9, 4268 **(2009)**.

Received: 19 May 2011. Accepted: 29 August 2012.